Fast Coherent Integration for Migrating Targets with Velocity Ambiguity

Stéphanie Bidon*, Laurent Savy†, François Deudon*
*Department Electronics Optronics and Signal, University of Toulouse/ISAE, Toulouse, France
Email: {sbidon,fdeudon}@isae.fr
†Radar and Electromagnetism Department, ONERA, Palaiseau, France
Email: laurent.savy@onera.fr

***Abstract*—In wideband radar, fast moving targets migrate through range gate during the coherent processing interval. To preserve coherent integration gain, range gate walk has to be taken into account. In this paper, we propose a fast algorithm based on a Keystone-like transform that allows one to perform such an integration in case of velocity ambiguous radar.**

I. Introduction

HIGH range resolution (HRR) radar systems will provide accurate measurement of range, target recognition and resistance to countermeasures [1]. Unlike classical low range resolution radars, HRR radars require large instantaneous bandwidth with respect to the carrier frequency. While it provides finer range cell and thus high range resolution features, it leads also to the well known range migration phenomenon. Indeed, moving targets, especially the fast one, may not be contained into a single range gate but migrate in range during the coherent processing interval (CPI). Therefore, range gate walk must be taken into account so as to preserve coherent integration gain [2].

The problem of range walk has been previously encountered for synthetic aperture radar (SAR) and inverse SAR (ISAR) applications. To address it, different methods have been proposed. Among them, the Keystone transform allows one to eliminate linear range migration regardless of the target velocity [3]–[6]. The principle of the transformation has been initially described in [3]. It consists of a one-dimensional interpolation of the signal in the fast-frequency/slow-time domain. More precisely, a slow-time rescaling is designed to remove cross-coupling terms that account for the range gate walk. In [4], [5], the authors propose to replace the interpolation algorithm of the Keystone transform by a method based on the scaling principle [7] that may be more convenient from a hardware point of view. In [8], a mapping similar to the Keystone transform has been proposed in the fast-frequency/slow-frequency domain to localize moving targets for ISAR imaging.

Unfortunately, all of these methods assume a non-ambiguous velocity mode and shall not be used in such case, e.g., for radar with low pulse repetition frequency (PRF). Instead, some authors have proposed to use the Keystone formatting while applying a correction factor that depends on the fold factor of the target Doppler [9]–[11]. In [9], [11], the fold factor is supposed to be known whereas in [10] a parallel searching scheme is proposed. The main drawbacks of these methods is the requirement of a high prior knowledge on the targets velocity and/or the inadequacy for multiple targets scenario.

In this paper, we propose a new fast algorithm based on a Keystone-like transform that performs coherent integration for wideband signals in case of velocity ambiguity. The transform can be applied independently for single-target or multi-target scenarios.

The following of the paper is organized as follows. In section II, the signal model for a wideband target is recalled. Then, in section III, the principle of the fast coherent integration is carefully explained. Numerical simulations are preformed in section IV to assess the performance of our new algorithm. Conclusions are given in section V.

II. Wideband signal model

In this section, we recall the signal model of a single point scatterer for wideband pulse radars [12]–[14]. The model is developed under the assumption that the range migration is negligible during the pulse width T but may be significant during the CPI. Also, a low PRF will be considered so that the radar is highly ambiguous in velocity but not in range. Note that, if carefully processed, range migration may allow one to alleviate the velocity ambiguity, so that the HRR radar will be neither ambiguous in range nor in velocity.

A. Signal model

1) Received signal: Consider a radar sending a series of M wideband pulses. The transmitted signal during one CPI is given by

$$s_{\text{tx}}(t) = \sum_{m=0}^{M-1} u(t - mT_R)e^{j2\pi f_0 t}$$

where $u(t)$ is the complex envelope with bandwidth B, T_R is the pulse repetition interval (PRI) and f_0 is the carrier

The work of F. Deudon is supported by the Délégation Générale pour l'Armement (DGA) and by Thales Systèmes Aéroportés.

frequency. The received signal echoed by a single scatterer can be expressed as

$$s_{\text{rx}}(t) = \alpha \sum_{m=0}^{M-1} u\left(t - mT_R - \tau(t)\right) e^{j2\pi f_0[t-\tau(t)]}$$

where α is the complex attenuation due to propagation and $\tau(t)$ is the round trip delay. In the following, the radial velocity v of the target is assumed to be constant over the CPI and much smaller than the wave propagation velocity c. Thus, the round trip delay can be considered as a linear function of time, i.e.,

$$\tau(t) = \tau_0 - \frac{2v}{c}t \quad \text{with} \quad \tau_0 = \frac{2R_0}{c}$$

where R_0 is the initial range of the moving scatterer. After downconversion, the received signal at the mth pulse can be written as[1]

$$s_{\text{rx}}(t', m) = \alpha\, u\left(t' - \left[\tau_0 - \frac{2v}{c} m T_R\right]\right) e^{j2\pi f_0 \frac{2v}{c}\left[t' + mT_R\right]} \tag{1}$$

where $t' = t - mT_R$ is the fast-time and the scatterer range has been assumed constant during the pulse duration, i.e.,

$$vT \ll \delta_R \quad \text{with} \quad \delta_R = \frac{c}{2B}.$$

In (1), the term $2vmT_R/c$ induces a translation of the envelope that may be significant over the CPI, i.e.,

$$vMT_R \gg \delta_R.$$

This term accounts for the range migration of moving scatterers. Note also that in (1), the classical phase shift from pulse to pulse is recovered.

2) Matched filtering: Traditionally, the received signal is matched filtered with the complex envelope of the transmitted signal $u(t)$. At the mth pulse, the output of the matched filtering can be expressed in the fast-time/slow-time domain as

$$\begin{aligned} x_{\text{ftst}}(t', m) &= \alpha\, e^{j2\pi f_0 \frac{2v}{c} mT_R} \\ &\quad \int u\left(y - [\tau_0 - \frac{2v}{c} mT_R]\right) e^{j2\pi f_0 \frac{2v}{c} y} u^*(y - t')dy \\ &= \alpha\, e^{j2\pi f_0 \frac{2v}{c} mT_R} e^{j2\pi f_0 \frac{2v}{c}\left[\tau_0 - \frac{2v}{c} mT_R\right]} \\ &\quad \int U\left(\nu - f_0 \frac{2v}{c}\right) U^*(\nu) e^{j2\pi\nu\left[t' - (\tau_0 - \frac{2v}{c} mT_R)\right]} d\nu \end{aligned}$$

where $U(\nu)$ is the Fourier transform of the complex envelope and the Parseval's theorem has been used as well as some standard properties of the Fourier transform. The expected range of targets velocity ensures both that the phase rotation due to the quadratic term $(2v/c)^2$ is negligible and that the following inequality is verified: $2vf_0/c \ll B$. Thus, the signal can be written as

$$\begin{aligned} x_{\text{ftst}}(t', m) &= \alpha\, e^{j2\pi f_0 \frac{2v}{c} mT_R} \\ &\quad \int |U(\nu)|^2 e^{j2\pi\nu\left[t' - (\tau_0 - \frac{2v}{c} mT_R)\right]} d\nu \end{aligned} \tag{2}$$

[1]Constant terms are systematically absorbed into α.

where one can recognize the inverse Fourier transform of the complex envelope spectrum.

3) Signal model in the fast-frequency/slow-time domain: According to (2), it appears natural to express the signal in the fast-frequency/slow-time domain [12]–[15]. Assuming that the spectrum of $u(t)$ is constant over the interval $[0, B[$ and null elsewhere, the Fourier transform of (2) with respect to the fast-time is given by

$$x_{\text{ffst}}(f, m) = \begin{cases} \alpha\, e^{j2\pi f_0 \frac{2v}{c} mT_R} e^{-j2\pi f\left[\tau_0 - \frac{2v}{c} mT_R\right)} \\ 0 \quad \text{if } f \notin [0, B[. \end{cases}$$

In a radar receiver, the Fourier transform is rather applied to discrete samples whose sampling rate is equal to $1/B$ in the fast-time dimension. In the following and without loss of generality, the moving scatterer is assumed to be completely entailed in the K first range gates. These K range gates define a low range resolution (LRR) segment that is of interest for our study. The discrete Fourier transform of the sequence $x_{\text{ftst}}(k/B, m)$ for $k = 0, \ldots, K-1$ can be approximated by

$$\boldsymbol{X}_{\text{ffst}}(k, m) = \alpha\, e^{j2\pi f_{d,t} m} e^{-j2\pi f_{r,t} k} e^{j2\pi\mu f_{d,t} mk} \tag{3}$$

where the fast-frequency $f_{r,t}$ and the Doppler frequency $f_{d,t}$ are respectively given by

$$f_{r,t} = \tau_0 \frac{B}{K} \quad \text{and} \quad f_{d,t} = f_0 \frac{2v}{c} T_R$$

and $\mu = B/(Kf_0)$ is a constant parameter that stands for the fractional bandwidth per subband. Note that the third exponential term in (3) accounts for the range migration.

B. Coherent integration

Performing the coherent integration for a signal whose signatures of interest are given by (3) amounts to derive

$$S(f_r, f_d) = \sum_{k=0}^{K-1} \sum_{m=0}^{M-1} \boldsymbol{X}_{\text{ffst}}(k, m) e^{-j2\pi m f_d (1+\mu k)} e^{j2\pi k f_r} \tag{4}$$

where

- f_r is the fast-frequency that spans the interval $[0, 1[$;
- f_d is the Doppler-frequency that spans the interval $[-n_{va}/2, n_{va}/2[$ where $n_{va} \in \mathbb{N}^*$ is the maximum Doppler ambiguity factor expected for a moving scatterer. In other words, if $v_{\max}$ denotes the maximum velocity expected for a target, n_{va} is the smallest integer that verifies $|v_{\max}| \leq n_{va}/2 \times v_a$.

While it allows to preserve the target gain, the sum (4) cannot be computed by a standard fast algorithm such as a two dimensional FFT. We present hereafter a method that allows one to compute rapidly (4).

III. Fast coherent integration algorithm

First, so as to motivate and comprehend the principle of the proposed algorithm, the signal model (3) is interpreted in four dual domains. Then, the fast coherent integration technique is described in details. Illustrations are given throughout this

TABLE I
SCENARIO PARAMETERS

Waveform		
carrier	$f_0 = 10$ GHz	
bandwidth	$B = 1$ GHz	
number of pulses	$M = 128$	
Processing		
LRR segment	$K = 128$	
unfolding factor	$n_{va} = 6$	
zero-padding	$n_{zp} = 4$	
interpolation	cubic spline	
Target		
velocity	$v = 18$ m/s	$f_{d,t} = 1.2$
initial range cell	$\tau_0 B = 80$	$f_{r,t} = 80/K$

section for a single moving scatterer. Scenario parameters are chosen according to an air-to-surface mode as depicted in Table I. Note that, given the parameters value, the ambiguous velocity $v_a = cf_r/(2f_0)$ is equal to 15 m/s. Useful processing parameters will be introduced throughout the section.

A. Representation of a target in dual domains

In this section, some insight is given to the target model (3). First let rewrite (3) as follows (with $\alpha = 1$)

$$\boldsymbol{X}_{\text{ffst}}(k,m) = e^{j2\pi f_{d,t} m} e^{-j2\pi k[f_{r,t} - \mu f_{d,t} m]} \quad (3\text{-}1)$$

$$= e^{j2\pi f_{d,t} m[1+\mu k]} e^{-j2\pi f_{r,t} k}. \quad (3\text{-}2)$$

Then let consider the four dual domains, i.e., the fast-time/slow-time, fast-time/slow-frequency, fast-frequency/slow-time, and fast-frequency/slow-frequency domains[2]. The modulus of the target amplitude is represented in these 4 domains in Fig. 1 and interpreted hereafter. The plots are obtained by applying standard fast Fourier transform (FFT) and inverse FFT (IFFT) operations to (3).

(a) According to (3-1), the target is localized in the fast-time/slow-time domain[3] on a line whose equation is given by

$$t_{\text{fast}}(m) = K\left[f_{r,t} - \mu f_{d,t} m\right] = \frac{R_0 - vT_R m}{\delta_R}.$$

The target is thus initially located at the range gate R_0/δ_R and then migrates of vT_R/δ_R range gates from pulse to pulse (see Fig. 1(a)).

(d) According to (3-2), the target is localized in the fast-frequency/slow-frequency domain, on a line whose equation is given by

$$f_{\text{na-slow}}(k) = f_{d,t}(1 + \mu k) = \frac{2v}{c} f_0 T_R + \frac{2v}{c}\frac{B}{K} T_R k. \quad (5)$$

The target slow-frequency is thus initially equal to the traditional Doppler frequency $f_{d,t}$ and then changes from subband to subband with a quantity equal to $\mu f_{d,t}$. Note that the subscript $_{na}$ in (5) refers to the non-aliased slow-frequency. Indeed, for low PRF radars, velocity ambiguity occurs and traditional spectral analysis such as an FFT lead to an aliased frequency[4] (see Fig. 1(d))

$$f_{\text{a-slow}}(k) = f_{\text{na-slow}}(k) \pm 0.5 n_k \quad (6)$$

where $n_k \in \mathbb{N}$ is the integer that ensures $f_{\text{a-slow}}(k) \in [-0.5, 0.5[$.

(b) In the fast-time/slow-frequency domain, the target response is spread over a rectangle having a height of $\Delta t_{\text{fast}} = -vMT_R/\delta_R$ and a width of $\Delta f_{\text{na-slow}} = 2vBT_R/c$ (see Fig. 1(b)). The faster the moving scatterer, the wider the spreading. Note that this rectangle might be aliased due to the velocity ambiguity.

(c) In the fast-frequency/slow-time domain, the modulus of the target amplitude is constant (see Fig. 1(c)).

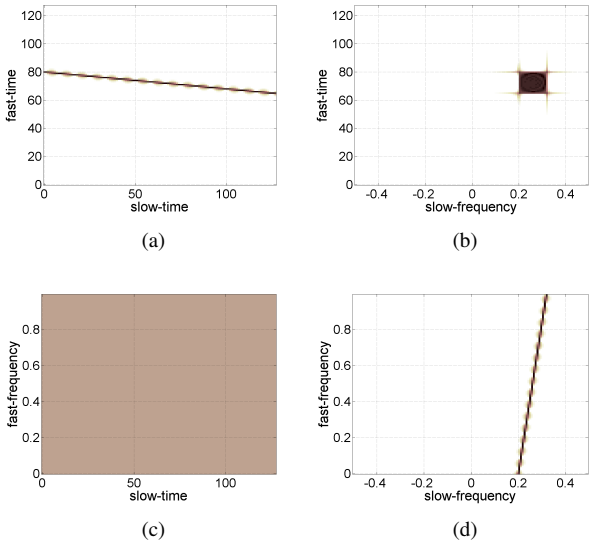

Fig. 1. Modulus of target amplitude. (a) Fast-time/slow-time domain. (b) Fast-time/slow-frequency domain. (c) Fast-frequency/slow-time domain. (d) Fast-frequency/slow-frequency domain.

Hereafter, we present an algorithm to derive (4) rapidly and show how the target locus is affected at each step of the method.

B. Details of the fast coherent integration

The whole processing is represented in the flowchart of Fig. 2. It consists mainly of unfolding the signal spectrum in the slow-frequency dimension thanks to an upsampling operation. Then, an inverse-Keystone transform is applied so as to realign the true target slow-frequency with respect to the fast-frequency. The method is illustrated in Fig. 3.

1) Upsampling: The first step of the algorithm is an upsampling operation. Once the data are obtained in the fast-frequency/slow-time domain, the slow-time sampling rate is increased by a factor of $n_{va} \in \mathbb{N}^*$. The output of the extender

[2]Fast-frequency bins are also denoted by the term subbands in this paper.

[3]For more convenience the fast-time is expressed as a range gate number.

[4]Slow-frequency interval will be centered around zero as the target velocity is a signed quantity.

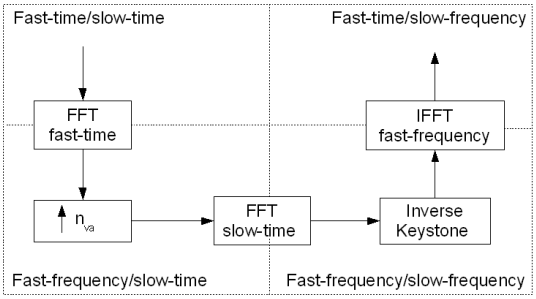

Fig. 2. Flowchart of the fast algorithm.

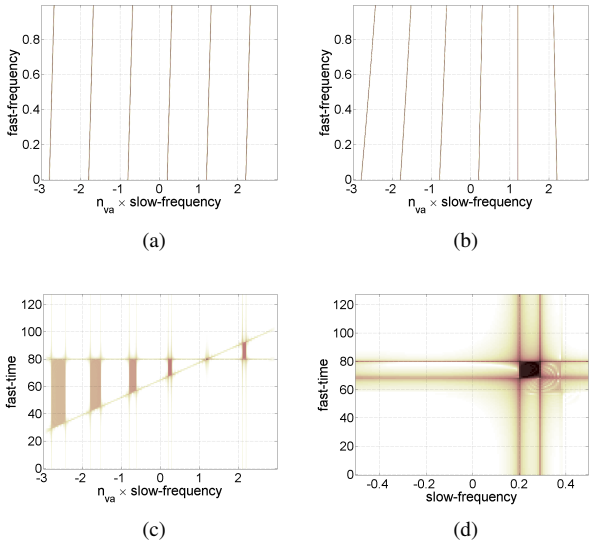

Fig. 3. Modulus of target amplitude. (a) Fast-frequency/slow-frequency domain after upsampling. (b) Fast-frequency/slow-frequency domain after inverse-Keystone mapping. (c) Fast-time/slow-frequency domain after IFFT. (d) Fast-time/slow-frequency domain after a Keystone transform.

is thus given, for $k = 0, \dots, K-1$ and $m = 0, \dots, \pm n_{va}M - 1$, by

$$\bar{\boldsymbol{X}}_{\text{ffsf}}(k,m) = \begin{cases} \boldsymbol{X}_{\text{ffst}}(k, \frac{m}{n_{va}}) & \text{if } m = 0 \pmod{n_{va}} \\ 0 & \text{otherwise.} \end{cases} \tag{7}$$

2) FFT on the slow-time: It is well known that the Fourier transform of the output (7) is a frequency-scaled version of the Fourier transform of the input [16]. Hence, using an M_{fft}-point FFT algorithm, one obtains for the kth subband

$$\begin{aligned} \bar{\boldsymbol{X}}_{\text{ffsf}}(k, f_{\text{slow}}) &= \sum_{m=0}^{M-1} \boldsymbol{X}_{\text{ffst}}(k,m) e^{-j2\pi m n_{va} f_{\text{slow}}} \\ &= \boldsymbol{X}_{\text{ffsf}}(k, n_{va} f_{\text{slow}}) \end{aligned} \tag{8}$$

where $f_{\text{slow}} \in [-0.5, 0.5[$ is in the discrete set

$$f_{\text{slow}} \in \left\{ \frac{0}{M_{\text{fft}}}, \frac{1}{M_{\text{fft}}}, \dots, 1 - \frac{1}{M_{\text{fft}}} \right\} - 0.5. \tag{9}$$

The orignal spectrum is thus unfolded by a factor n_{va}. As depicted in Fig. 3(a), the locus of a single scatterer and those of its pth ghost are described by lines whose equations are respectively given by

$$\begin{aligned} n_{va} f_{\text{na-slow}}(k) &= f_{d,t} + \mu f_d k \\ n_{va} f_{\text{na-slow}}(k) &= f_{d,t} + p + \mu f_d k \quad \text{with } p \in \mathbb{Z}^*. \end{aligned}$$

3) Inverse-Keystone transform: The next step of the algorithm aims at realigning the target spectrum in the slow-frequency dimension. To do so, we propose to perform an inverse-Keystone transform that rescales the slow-frequency axis regardless of the target features, i.e., at each subband k the spectrum (8) is derived at the points

$$(1 + k\mu) f_{\text{slow}}. \tag{10}$$

As the frequency axis is dilated, one has to avoid any extrapolation by discarding the points that do not verify $(1 + k\mu) f_{\text{slow}} \in [-0.5, 0.5[$. Interpolated frequency points are represented in Fig. 4. After the inverse-Keystone mapping, (8) becomes

$$\bar{\boldsymbol{X}}_{\text{ffsf}}(k, (1+k\mu) f_{\text{slow}}) = \sum_{m=0}^{M-1} \boldsymbol{X}_{\text{ffst}}(k,m) e^{-j2\pi m (1+k\mu) n_{va} f_{\text{slow}}}.$$

It is essential to note that (10) can be performed via a fast interpolation algorithm as the linear or the cubic spline interpolation methods [17]. Naturally, zero-padding is thus required while deriving (8) to obtain satisfying results (e.g., a factor of 4 per ambiguity interval). As discussed later, the choice of the zero-padding factor as well as the interpolation technique is a compromise between the computational complexity and the convergence rate.

As depicted in Fig. 3(b), the locus of a single scatterer and those of its pth ghost are given respectively by

$$n_{va} f_{\text{na-slow}}(k) = f_{d,t} \tag{10a}$$

$$\begin{aligned} n_{va} f_{\text{na-slow}}(k) &= f_{d,t} + \frac{p}{1 + \mu k} \\ &\approx [f_{d,t} + p] - p\mu k. \end{aligned} \tag{10b}$$

where $p \in \mathbb{Z}^*$. Note that the former describe a vertical line (10a) while the latter can be approximated by a line (10b) with slope $-p\mu$.

4) IFFT on fast-frequency: The last step of the algorithm consists of a simple IFFT. As the target spectrum is realigned in the slow-frequency according to (10a), one only needs to sum coherently the samples with respect to the fast-frequency dimension to localize the target in range. The IFFT output is given by

$$\begin{aligned} \bar{\bar{\boldsymbol{X}}}_{\text{ftsf}}(f_r, f_{\text{slow}}) &= \sum_{k=0}^{K-1} \bar{\boldsymbol{X}}_{\text{ffsf}}(k, (1+k\mu) f_{\text{slow}}) e^{j2\pi k f_r} \\ &= S(f_r, n_{va} f_{\text{slow}}) \end{aligned} \tag{11}$$

with $f_r \in [0, 1[$ and where one recognize the sum (4) with $f_d = n_{va} f_{\text{slow}}$. As depicted in Fig. 3(c), the traditional "butterfly" shape is recovered [15]. The locus of a single scatterer is a peak located at the position $(K f_{r,t}, f_{d,t})$ while those of its ghosts describe approximately rectangles located

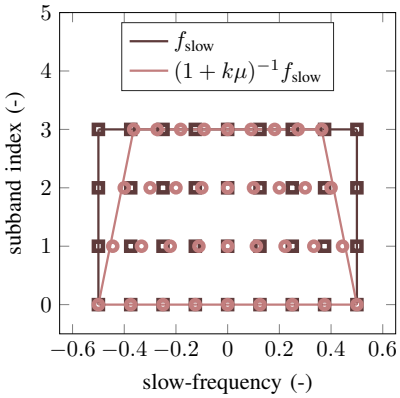

Fig. 4. Interpolated frequency points for the inverse Keystone transform. (Numerical values of the scenario parameters have been changed for illustrative purpose.)

at the position $(Kf_{r,t}, f_{d,t}+p)$ and having a height and a width respectively given by

$$\Delta t_{\text{fast}} = p(B/f_0)M \tag{11a}$$

$$\Delta n_{va} f_{\text{na-slow}} = -pB/f_0. \tag{11b}$$

Note that height and width (12) do not depend on the target features but correspond to those of a target with velocity pv_a. Same remark applies to the sidelobes level. Indeed, if there is only one target in the data, one can show that

$$|S(f_{r,t}, f_{d,t})| = KM \tag{11c}$$

$$|S(f_{r,t}, f_{d,t}+p)| \approx K\frac{1}{p}\frac{f_0}{B}. \tag{11d}$$

In other words[5], the relative sidelobe level at the pth velocity ambiguity is equal to $1/p \times f_0/(MB)$. This quantity is actually the inverse of (11a), that stands for the migration—expressed in cell range—of a scatterer with velocity pv_a during the whole CPI.

Finally, for comparison purposes, Fig. 3(d) illustrates the inefficiency of a simple Keystone transform in case of velocity ambiguity.

IV. Performance

Herein we analyse the performance of the new algorithm described in section III. More precisely, we are interested in the computational complexity and the convergence rate of the approximated sum (11).

- Computational complexity of (11) is assessed via the computational time and is compared to the one required to derive the exact sum (4). For a fair comparison, the sum on the subband index k is performed via a K-point IFFT in both cases.
- Convergence rate of (11) is assessed via the relative error between the exact sum (4) and the approximated sum (11).

[5](11d) is a coarse approximation.

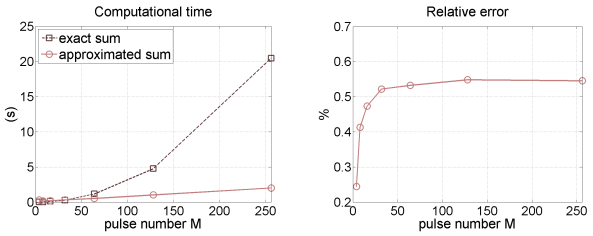

(a) (b)

Fig. 5. Influence of pulse number M. (a) Computational time. (b) Relative error of the approximated sum.

To compare precisely (4) and (11), both sums are derived for the frequency points $f_d = n_{va} f_{\text{slow}}$ where f_{slow} is described by (9). We recall that zero-padding is performed while deriving (8), so that the FFT-point number can be written as

$$M_{\text{fft}} = n_{zp} n_{va} M \tag{12}$$

where n_{zp} stands for the zero-padding factor per velocity ambiguity. Given (9) and (12), the slow-frequency points of interest are thus

$$f_d \in \left\{0, \frac{1}{n_{zp}M}, \ldots, n_{va} - \frac{1}{n_{zp}M}\right\} - \frac{n_{va}}{2} \tag{13}$$

Also, we discard in (13) frequency points for which $(1+(K-1)\mu)f_{\text{slow}} \notin [-0.5, 0.5[$. Numerical simulations have been performed with the Matlab software. Note that parameters of the target have been changed in this section to $v = 0$ and $\tau_0 B = K/2$. Otherwise stated, parameters used are those described in Table I. More precisely, in the following paragraphs, parameters of interest are varied one at a time.

A. Influence of the pulse number M

According to Fig. 5, the computational time of the proposed algorithm varies slowly with respect to the number of pulses whereas the time required for an exact sum increases drastically. Note that the proposed algorithm can be qualified as "fast" beyond a certain number of pulses (here $M \approx 32$). For a radar scenario, this may be always the case. Finally, the number of pulses M does not affect greatly the accuracy of the approximated sum (11).

B. Influence of the unfolding factor n_{va}

The influence of the unfolding factor n_{va} is illustrated in Fig. 6. The computational time of the proposed algorithm increases slowly with respect to the unfolding factor whereas it increases rapidly for the exact sum (4). Also, the accuracy of our method is barely affected by the unfolding factor. Note that it is all the more interesting that the range-velocity map is unfolded.

C. Influence of the zero-padding factor n_{zp}

We study here the influence of the zero-padding factor n_{zp}. On one hand this factor will improve the interpolation accuracy thus the convergence of the proposed algorithm; on the other hand it increases the number of slow-frequency points hence it

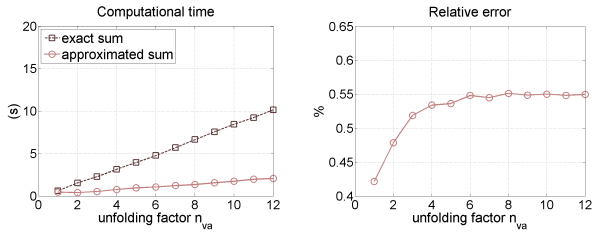

(a) (b)

Fig. 6. Influence of the unfolding factor n_{va}. (a) Computational time. (b) Relative error of the approximated sum.

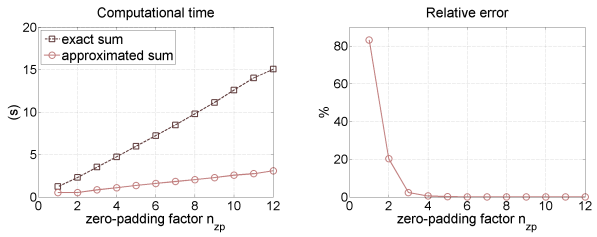

(a) (b)

Fig. 7. Influence of the zero-padding factor n_{zp}. (a) Computational time. (b) Relative error of the approximated sum.

will increase the computational time. These trends are clearly recovered in Fig. 7. However, with our proposed method, the computational time increases slowly compared with the computational time needed for an exact sum. Also, the relative error of (11) decreases very rapidly with respect to n_{zp}. Here a factor $n_{zp} = 4$ seems to be a good compromise between computational complexity and accuracy (i.e., the relative error is less than 1% and the computational time is about 1.15s).

D. Influence of the interpolation algorithm

Finally, we study the influence of the interpolation algorithm chosen to perform the inverse-Keystone transform (10). We recall here that samples used for interpolation are complex data equally spaced according to (9). More precisely, the sampling increment is given by $1/M_{\text{fft}} = 1/(n_{zp}n_{va}M)$. In the following, we compare performance of the cubic spline method with the one of the linear interpolation when the sampling increment is increased via the zero-padding factor n_{zp}. Results are depicted in Fig. 8. As expected, the accuracy is increased with the cubic spline method but at the price of a higher computational complexity. It belongs then to the radar designer to make a compromise regarding these two aspects.

V. Conclusion

In this paper, we have proposed a new fast algorithm that allows one to integrate coherently migrating targets in case of velocity ambiguity. The procedure takes into account linear range migration and is based on an inverse-Keystone transform. Performance of the method has been studied and showed that the algorithm is computationally efficient and accurate. This algorithm could be used directly for detecting

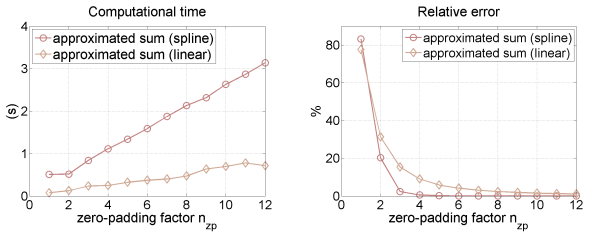

(a) (b)

Fig. 8. Influence of interpolation method. (a) Computational time. (b) Relative error of the approximated sum.

migrating targets or it could be part of more complex detection schemes.

References

[1] M. I. Skolnik, *Radar Handbook*, 3rd ed. McGraw-Hill, 1970.

[2] D. C. Lush and D. A. Hudson, "Ambiguity function analysis of wideband radars," in *Proc. 1991 IEEE National Radar Conf.*, Los Angeles, CA, USA, Mar. 12–13, 1991, pp. 16–20.

[3] R. P. Perry, R. C. DiPietro, and R. L. Fante, "SAR imaging of moving targets," *IEEE Trans. Aerosp. Electron. Syst.*, vol. 35, no. 1, pp. 188–200, Jan. 1999.

[4] D. Zhu, Z. Zhu, and L. Wang, "SAR ground moving target imaging based on Keystone transform without interpolation," in *Proc. IEEE IGARSS*, Seoul, Korea, July 25–29, 2005, pp. 20 946–2948.

[5] D. Zhu, Y. Li, and Z. Zhu, "A Keystone transform without interpolation for SAR ground moving-target imaging," *IEEE Geosci. and Remote Sensing Lett.*, vol. 4, no. 1, pp. 18–22, Jan. 2007.

[6] M. Xing, R. Wu, J. Lan, and Z. Bao, "Migration through resolution cell compensation in ISAR imaging," *IEEE Geosci. Remote Sensing Lett.*, vol. 1, no. 2, pp. 141–144, Apr. 2004.

[7] A. Papoulis, *Systems and Transforms with Application in Optics*. New-York: McGraw-Hill, 1968.

[8] M. Soumekh, *Fourier Array Imaging*. Engledwood Cliffs, New Jersey: Prentice Hall, 1994.

[9] S.-S. Zhang, T. Zeng, T. Long, and H.-P. Yuan, "Dim target detection based on Keystone transform," in *Proc. IEEE Int. Radar Conf.*, May 9–12, 2005, pp. 889–894.

[10] Y. Li, T. Zeng, T. Long, and Z. Wang, "Range migration compensation and Doppler ambiguity resolution by Keystone transform," in *Proc. IEEE Conf. on Radar*, Shanghai, Oct. 16–19, 2006, pp. 1–4.

[11] R. P. Perry, R. C. DiPietro, and R. L. Fante, "Coherent integration with range migration using Keystone formatting," in *Proc. IEEE Int. Radar Conf.*, Apr. 17–20, 2007, pp. 863–868.

[12] T. J. Abatzoglou and G. O. Gheen, "Range, radial velocity, and acceleration MLE using radar LFM pulse train," *IEEE Trans. Aerosp. Electron. Syst.*, vol. 34, no. 4, pp. 1070–1084, Oct. 1998.

[13] N. Jiang, R. Wu, and J. Li, "Super resolution feature extraction of moving targets," *IEEE Trans. Aerosp. Electron. Syst.*, vol. 37, no. 3, pp. 781–793, July 2001.

[14] F. Deudon, S. Bidon, O. Besson, J.-Y. Tourneret, M. Montécot, and F. Le Chevalier, "Modified Capon and APES for spectral estimation of range migrating targets in wideband radar," in *Proc. IEEE Int. Radar Conf.*, May 10–14, 2010.

[15] F. Le Chevalier, *Principles of Radar and Sonar signal processing*. Norwood, MA: Artech House, 2002.

[16] A. V. Oppenheim and R. W. Schafer, *Discrete-time Signal Processing*. Prentice Hall, 1989.

[17] C. de Boor, *A Practical Guide to Splines*. Springer-Verlag Berlin and Heidelberg GmbH & Co. K, 1978.